Solar Energy Materials & Solar Cells 113 (2013) 171–178

Contents lists available at SciVerse ScienceDirect

Solar Energy Materials & Solar Cells

journal homepage: www.elsevier.com/locate/solmat

Factors limiting the doping efficiency of transparent conductors: A case study of Nb-doped In_2O_3 epitaxial thin-films

O. Lozano [a,b,1], Q.Y. Chen [a,b,*], P.V. Wadekar [a,b], H.W. Seo [c], P.V. Chinta [a,b,2], L.H. Chu [a,3], L.W. Tu [b], Ikai Lo [b], S.W. Yeh [d,4], N.J. Ho [d], F.C. Chuang [b], D.J. Jang [b], D. Wijesundera [a], Wei-Kan Chu [a]

[a] Department of Physics, Texas Center for Superconductivity, University of Houston, Houston, TX 77204, USA
[b] Department of Physics, Center for Nanoscience and Nanotechnology, National Sun Yat-Sen University, Kaohsiung 80424, Taiwan
[c] Department of Physics, University of Arkansas, Little Rock, AR 72204, USA
[d] Department of Materials and Optoelectronic Science, Center for Nanoscience and Nanotechnology, National Sun Yat-Sen University, Kaohsiung 80424, Taiwan

ARTICLE INFO

Article history:
Received 24 July 2012
Received in revised form
24 January 2013
Accepted 4 February 2013
Available online 16 March 2013

Keywords:
Transparent conducting oxide
Indium oxide
Niobium doping
Epitaxial thin film
Highly transparent

ABSTRACT

In_2O_3 epitaxial thin films with heavy Nb doping have been investigated in expectation of achieving higher doping efficiency per doping atom than what has been achieved by Sn-doping because Nb has one more available valence electron. The films were deposited by co-sputtering of Nb and In_2O_3 on (001) YSZ substrates, and are found to follow the epitaxial relations of $[001]In_2O_3||[001]$YSZ and $[110]In_2O_3||[110]$YSZ aligned within $\Delta\omega\sim0.31$–0.41° of full rocking width at half maximum (FWHM). The doped thin films present optical transparencies of 97–99 % with electrical resistivities down to $10^{-4}\,\Omega$ cm, 100 times lower than the as-deposited pristine thin films of no intentional doping. Optimal doping efficiency of $\eta_{max}\sim1$ charge carrier per Nb-atom added, not the hoped 2, suggests an effective ionization state of $Nb^{\bullet}_{In}$, much like $Nb^{\bullet}_{Sn}$, rather than the anticipated $Nb^{\bullet\bullet}_{In}$. This singly-charged state is associated with the formation of Nb_2O_4 molecules by drawing extra interstitial O_i atoms to gather around the substitutional Nb_{In} sites, as confirmed by XPS based on the chemical-shift of the X-ray photoelectron energy that measures the binding energy of core–shell electrons. Plasma oscillation analysis by FTIR optical spectroscopy shows an anomalously-high effective mass, about 10 times larger than the reported $m^*=0.35m_e$. A dual-band model is proposed to reconcile with the findings.

© 2013 Elsevier B.V. All rights reserved.

1. Introduction

Host compound semiconductor of composition $A_p^{+m}O_{mp/2}^{-2}$ doped with atoms of valence-q should, in principle, acquire as many as $n=q-m$ charged-carriers per dopant upon substitution of the cation A. Heavy doping of valence-5 Nb-atoms into In_2O_3, for example, may provide two free carriers per Nb doped, yielding a doping efficiency of $\eta_{max}=2$. This was expected to contrast $\eta_{max}=1$ for the widely-used transparent conducting oxides (TCOs) of indium-tin oxide (ITO) in which Sn of valence-4 is used. In this work, however, such simple inference was found false based on the evidences of oxometalates formation, such as Nb_2O_4 for the Nb dopants, and likely partial formation of Sn_2O_4 as well for the ITO, all showing compromised doping efficiency.

TCOs are a class of semiconductors which become highly conductive upon heavy doping but remain optically transparent. Such materials have found increasing uses in devices such as flat panel displays (FPD), light-emitting devices (LEDs), solar cells, and architectural windows [1]. In_2O_3 is a widely-used industrial TCO material due to its low resistivity and high optical transparency after tin-doping (ITO) [2,3]. As ITO is becoming a popularly used industrial material, the massive use of tin has caused some environmental concerns. Hence, there indeed is an incentive to look for alternative TCOs of equal or even better performance. While some success has been achieved, including W:In_2O_3 [4], Zr:In_2O_3 [5], InGaO [6], and InZnO [7], the underlying physics of a good TCO remains largely an under-cultivated field. For example, it is not clear why most TCOs receive less than one free carrier for each dopant introduced. For a semiconductor to be transparent, it is first required to have a band gap E_g larger than the photon energy of the visible light, or about 380 nm on the short end of the wavelength range. Oxides thus are natural candidates as many of them have an E_g that is large enough. To make a wide-bandgap semiconductor conductive, however, one must

* Corresponding author.
E-mail addresses: qchen@faculty.nsysu.edu.tw, qchen@uh.edu (Q.Y. Chen).
[1] Now at Laboratory of Analyses by Nuclear Reactions, University of Namur, Belgium.
[2] Now at Department of Physics and Materials Science Program, University of Vermont, Burlington, VT 05405, USA.
[3] Now at Taiwan Semiconductor Manufacturing Company, Hsin Chu 30077, Taiwan.
[4] Now at Metals Industry Development Center, 1001 Kao-Nan Highway, Kaohsiung 81160, Taiwan.

0927-0248/$ - see front matter © 2013 Elsevier B.V. All rights reserved.
http://dx.doi.org/10.1016/j.solmat.2013.02.006

bring in enough free charge carriers, typically by extrinsic doping to introduce impurity states sufficiently near the edges of conduction band (CB) or valence band (VB) in order for thermal activation to be effective. In fact, the doping level typically would have to be so high that energy states of impurities could form into a band that overlaps with the CB or VB of the host semiconductor. The upper end of such impurity band then constitutes the Fermi level within the conduction band (for n-type) or valence band (for p-type) of the degenerate semiconductor. In reaching desired high electrical conductivity, one is expected to seek optimal product of carrier concentration and mobility, namely, $n\mu_n$ or $p\mu_p$ as $\sigma=(n\mu_n+p\mu_p)e$, with e representing the fundamental charge of 1.6×10^{-19} C. However, the decrease in mobility, $\mu=e\tau/m^*$ in the simple context of Drude approximation, due to the increased scattering rate of $1/\tau$ as the doping level increases, eventually will offset what is gained from the increase in density of free carriers in their combined contribution to increasing conductivity. Finally, the effective mass of carriers must also be taken into account, though this is a matter mostly of the host semiconductor rather than that of the dopant. The picture described above alludes to the complexity in acquiring a simple tailor's rule for TCOs. In order to provide a better strategy on the material search, the transport properties must be studied as a function of temperature and doping levels on a larger pool of semiconductors of wide-bandgap with proper band-edge dopant states. This work was indeed motivated by such intention using Nb-doping of In_2O_3 as a case in point.

One plausible path to enhancing electrical conductivity, as discussed above, is by use of a donor dopant which could provide more than one free electron carrier per substitution of the host atom, such as by Nb^{+5} rather than by Sn^{+4}, when substituting In^{+3}. This is seen from the ground state electron configuration of [Kr] $4d^{10}$ $5s^2$ $5p^2$ for the Sn-atoms in place of [Kr] $4d^{10}$ $5s^2$ $5p^1$ for indium in In_2O_3, where it is replaced with [Kr] $4d^4$ $5s^1$ for Nb, would in principle contribute to the doping effect. If any of the Sn dopants should form into SnO_2, that particular Sn atom would have no free carrier to contribute. By the same token, though Nb has five valence electrons available, if Nb_2O_5 should ever form, the specific atom would not contribute as a donor either. However, while Nb_2O_5 is the most stable among all oxides of Nb, NbO, Nb_2O_3, Nb_2O_4, and Nb_2O_5 can all exist as stable compounds, thus the effectiveness of doping would likely depend on the dominating oxidation state, which is also a subject matter of this paper.

We sought epitaxy in this work lest spurious effects of structural defects, such as grain boundaries, should overshadow the intrinsic behaviors we want to investigate. Except for a few cases, including Nb:TiO_2 [8], Ga:ZnO [9], and Al:ZnO [10], variable-temperature magneto-transport behaviors of the TCOs have rarely been extensively studied despite their close correlation with the mechanisms of electric conduction. In what follows, we report on the crystal structure, temperature dependent magneto-transport, optical properties, and chemical analysis of epitaxial thin-film samples, obtained via co-sputtering, with nominal Nb contents ranging from 0.7 to 9.1 at%. We seek to explore how the extra valence charge of Nb atoms would contribute to the charge carrier transport in comparison with the single charge from Sn, and how the underlying charge scattering would play out in the making of a transparent conductor using a wide-bandgap semiconductor.

2. Experimental details

A co-sputtering system, consisting of an RF and a DC gun, set orthogonal to each other, with the substrate holder placed at 45° with respect to both, was used. The RF gun was loaded with a 99.99% pure In_2O_3 target, 2 in. in diameter, while the DC gun with a 99.95% pure Nb target of similar dimensions. Doping levels were regulated by varying the DC power. All films were grown at 550 °C substrate temperature, providing optimal crystalline quality and lowest resistivity. The base vacuum pressure was lower than 5×10^{-7} Torr, while during deposition the working pressure reached 66 mTorr after introducing flowing Ar regulated by a mass flow controller. Crystal quality was measured with D5000 and D1 X-ray diffractometers (XRD) using the Cu K-α lines. Surface morphology was measured with an atomic force microscope (AFM) (Dimension 3100, Digital Instruments). Dopant concentration and thickness were measured by RBS and PIXE on an ion beam facility. Magneto-transport measurements were done using a six-probe Hall-bar configuration on a Lakeshore 7500 Hall measurement system. Optical properties were measured in the UV to near-IR range with an Ultrospec 2100 Pro spectrophotometer up to the near-IR, while mid-IR was measured with a Bruker Vertex 70 V Fourier-transform spectrophotometer. In order to investigate the chemical bonding, XPS chemical analysis was done on a Physical Electronics PHI 5700 ESCA system with an Al filament.

3. Results and discussion

3.1. Structural characterization

In_2O_3 of bixbyite structure has 80 atoms per unit cell with lattice parameter $a=10.118$ Å [11]. Substrates of (001)-cut yttria-stabilized zirconia (YSZ), assuming fluorite structure with $a=5.133$ Å, provide an excellent 2:1 coincidence lattice match with $a_{film}\approx2a_{substrate}$. Fig. 1 shows the 2θ XRD patterns of the $In_{2(1-x)}Nb_{2x}O_3$ films with $x=0\%$, 0.7%, and 9.1% grown on (001)-YSZ substrates, with the thickness ranging from 200 to 300 nm. Only the In_2O_3 (00$2l$) and substrate (00l) peaks are present, demonstrating excellent phase purity and film–substrate alignment of (001)In_2O_3||(001)YSZ. The in-plane alignment was analyzed by XRD through comparing 360° ϕ-scans of (111) YSZ and (222) In_2O_3 peaks. This gives [$\bar{1}$10]In_2O_3||[$\bar{1}$10]YSZ as the two peaks of different 2θ angles would appear at the same ϕ-angles when their [$\bar{1}$10] zone axis, which is common to the (001) and (111) planes of both the In_2O_3 films and YSZ substrates, is parallel to the plane of incidence spanned by the incoming and diffracted X-rays. The narrow widths of rocking curves suggest reasonable crystalline quality. In the upper insets of Fig. 1, the ω-scans around the [$\bar{1}$10] axis, viz. the rocking curves of the (004) and (222) peaks for the $x=0.7\%$ films show a FWHM of 0.39° (004) and 0.36° (222), respectively, corroborating the asserted epitaxial nature of the film. The In_2O_3 (004) ω-rocking curve shows a decrease in its FWHM with increasing Nb-doping: 0.54° for $x=0\%$ to 0.39° for $x=0.7\%$, then 0.40° at $x=3.2\%$, before dropping down to 0.28° for $x=4.2\%$ and 0.30° for $x=9.1\%$. These values are listed in Table 1. The improvement of structural perfection reflected in reduced width of rocking curves after Nb-doping suggests that the Nb atoms help stabilize the overall host In_2O_3 structure, possibly by drawing in oxygen to form Nb_2O_4 in some Nb_{In} sites, which then augments the effective size of the substituted atom. To support this assertion, we observe that the change in lattice parameter due to doping, as shown in Table 1, is minimal, even though the ionic size of Nb^{+5} is ~15–20% smaller than that of In^{+3}. That is, the doping does not affect the structural integrality of samples, although heavy doping does result in lattice imperfections that contribute to the overall variations in crystallinity. The middle insets compare the surface morphology as determined by the atomic force microscopy (AFM) for

x=0%, 0.7%, and 3.2%, from which the increases in Nb-doping are seen to cause increasingly rougher surfaces. Note that this increased roughness, interpreted as a result of island growth, occurs concurrently with the reduced width of rocking curve. Island formation provides a path to strain relaxation, which is largely dictated by the intricate balance between the surface energy and chemical bonding, for example, with the strain energy built up during the thin film growth.

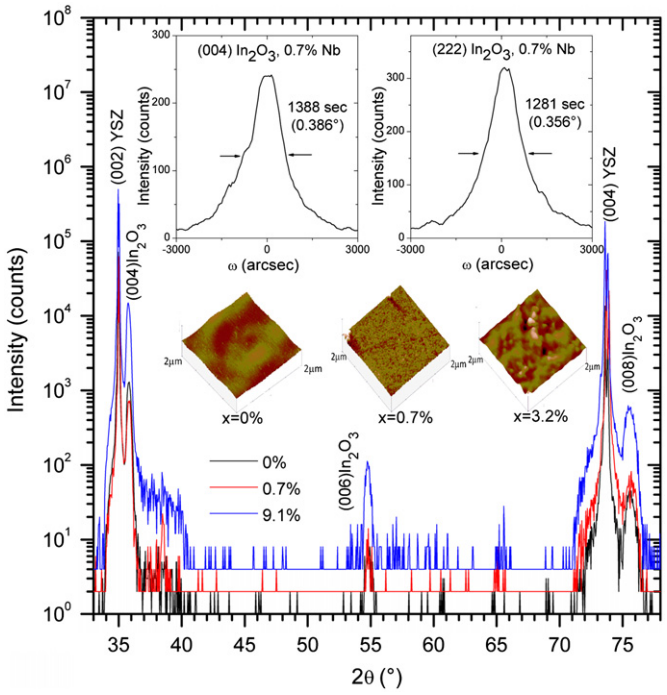

Fig. 1. XRD θ–2θ patterns for (00l) oriented $In_{2(1-x)}Nb_{2x}O_3$ epitaxial films doped with Nb for x=0%, 0.7% and 9.1%, indicating no detectable spurious phases. Upper left inset: rocking curve of (004) In_2O_3 peak around [$\bar{1}$10] for x=0.7% Nb. Upper right inset: the rocking curve of (222) In_2O_3 peak around [$\bar{1}$10] for x=0.7% Nb. Middle insets: AFM topographic scans of the Nb-doped In_2O_3 samples with x=0%, 0.7% and 3.2%. Z-axis scales: 20 nm for x=0%, 40 nm for x=0.7% and 3.2%. Each topographic scan is 2×2 μm^2.

3.2. Magneto-transport properties

Temperature-dependent resistivity $\rho(T)$, carrier concentration $n(T)$, and Hall mobility $\mu_H(T)$, are presented in Fig. 2. The inset of Fig. 2(a) shows $\rho(T)$ of all samples. The most resistive film was the pristine In_2O_3, with $\rho(300\,K)\approx56$ mΩ cm and $\rho(4\,K)\approx112$ mΩ cm. It has a negative temperature coefficient of resistance (TCR) that is characteristic of semiconductor. Nevertheless, since the ratio of $\rho(4\,K)/\rho(300\,K)$ is only about two for the sample without doping, while for typical semiconductors this value is orders of magnitude larger, thus pristine films already are highly doped, most likely due to intrinsic point defects. This will be further discussed below in the section on optical properties where the Fermi levels of samples are found to lie in the conduction band. The incorporation of Nb led to drastic changes in the transport properties. The resistivity decreased up to 100 times, reaching $\rho(300\,K)=4.1\times10^{-4}$ Ω cm for x=3.2%, close to the reported $1–3\times10^{-4}$ Ω cm for typical ITO thin films [12–15]. Further increase in Nb-doping eventually reached a bottleneck, as judged by the resistivity increment. The normalized resistivity data $\rho_N(T)$, shown in Fig. 2(a) as

$$\rho_N(T)=[\rho(T)-\rho_{min}]/[\rho_{max}-\rho_{min}] \quad (1)$$

demonstrate a metal-like positive TCR at high temperatures. At lower temperatures the dopant impurities led to a change from positive to negative TCR as the temperature decreases, as shown in Fig. 2(a). This change of TCR at low temperatures, which has also been observed in other heavily-doped TCO systems such as Nb:TiO_2 [8], Ga:ZnO [9], Al:ZnO [10], and other epitaxial films of ZnO [16,17], is a signature of carrier scattering in disordered electronic systems [18], generally categorized in literature as weak localization of charge carriers. Note for x=3.2%, this sign change of TCR is the least obvious, but the Hall mobility is highest. It is not clear, however, whether the occurrence of a change of TCR requires the carrier mobility to be smaller than a threshold value, but the $-\ln T$ dependence in the negative TCR region, as to be discussed below, does indeed appear to link the behaviors to weak localization of the carriers [18]. Analysis of the resistivity curves has been made with variable range hopping (VRH) electric

Table 1
Parameters of the Nb-doped In_2O_3 films.

Nb (at%)→	0	0.7	3.2	4.2	9.1
Rocking $\Delta\omega$ FWHM (004) (deg.)	0.54	0.39	0.4	0.28	0.3
Lattice parameter (Å)	10.05	10.05	10.07	10.04	10.05
Hall carrier conc., n_{Hall} (300 K) [cm^{-3}]	1.77×10^{20}[a]	2.38×10^{20}	8.66×10^{20}	1.68×10^{21}	1.89×10^{21}
Optical carrier conc., n_{opt} (300 K) [cm^{-3}][b]	3.01×10^{18}	2.89×10^{19}	7.84×10^{19}	1.62×10^{20}	1.76×10^{20}
Optical gap, $E_{g\ opt}$ (eV)	3.66	3.67	3.78	3.88	3.92
Fermi level (eV)[c]	0.76	0.77	0.88	0.98	1.02
Hall mobility (300 K) (cm^2/Vs)	0.62	13.48	17.40	0.27	2.29
Optical mobility (300 K) (cm^2/Vs)	19.78	23.57	34.58	10.94	3.98
Plasma frequency (s^{-1})[d]	8.26×10^{13}	2.56×10^{14}	4.12×10^{14}	6.06×10^{14}	6.32×10^{14}
Effective electron mass (m_e)[e]	20.64	2.89	4.06	3.64	3.77
Effective electron mass near E_f (m_e)[f]	0.15	0.18	0.38	0.53	0.55
Θ_D (K)	n/a	195	210	163	185
Doping efficiency (%)	n/a	26	66	97	59

[a] Calculated from extrapolation based on the Burstein–Moss shift.
[b] Assuming constant effective mass m=0.35m_e.
[c] Using E_g=2.9 eV.
[d] Using Eq. (5).
[e] Replacing n_{opt} with n_{Hall} in Eq. (6).
[f] Substituting n with n_{Hall} in Eq. (4).

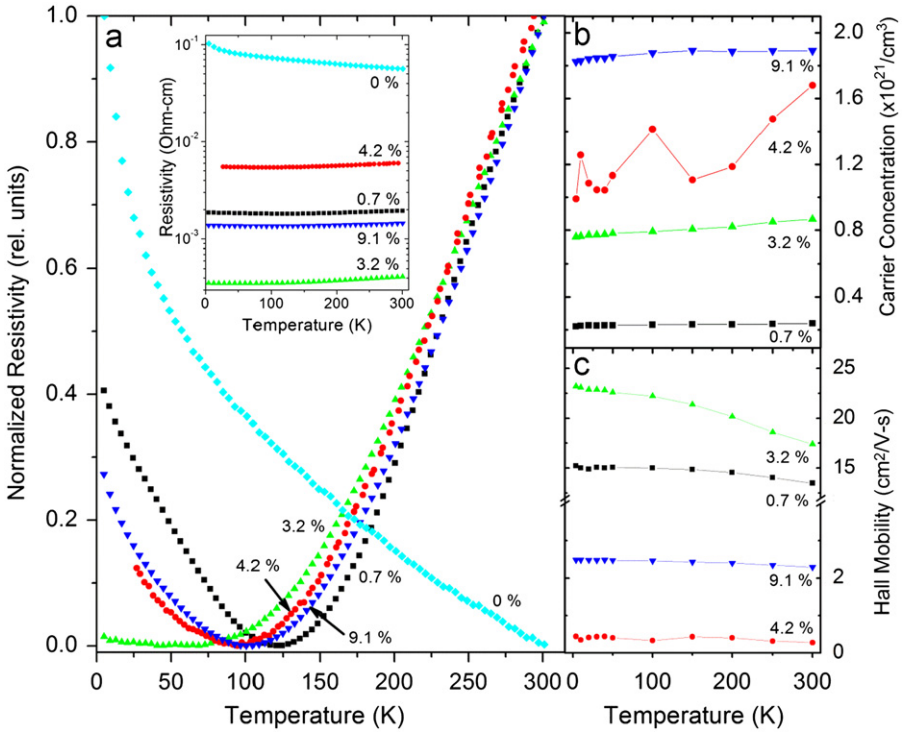

Fig. 2. (a) Normalized resistivity calculated with Eq. (1), (b) carrier concentration, and (c) Hall mobility as a function of temperature. The inset in (a) shows the resistivity plots as a function of temperature.

conduction mechanism. This mechanism is described in [19] as

$$\rho(T) = \rho_0 \exp\left[\left(\frac{T_0}{T}\right)^m\right] \tag{2}$$

where ρ_0 is the intrinsic resistivity, T_0 the activation temperature, and $m=1/(1+d)$ where d is the system dimensionality. The resistivity curves were fitted in Fig. 3 with the VHR mechanism, using $m=1/4$ (three dimensional scenario). The activation temperatures T_0 were found to be 2.34×10^{-3}, 4.1×10^{-9}, 1.46×10^{-4}, 6.56×10^{-5} K for samples $x=0.7\%$, 3.2%, 4.2%, and 9.1%, respectively. These activation temperatures are markedly lower than those found for In_2O_3 wires [20], but simple fittings are good obviously only for $x=3.2\%$ and 4.2%. The exact nature of the electrical behaviors needs to be further investigated since, as shown in Fig. 3(b), a scenario based on weak localization is also likely for the log T dependence [16].

The small positive temperature derivative of carrier concentration $dn(T)/dT$, shown in Fig. 2(b), agrees with the typical minimal semiconducting thermal activation dependence of degenerate semiconductors which would exhibit positive TCR. Physically, metal atomic dopants at high concentration would form an impurity band overlapping with the conduction band of the host In_2O_3 [2], making its conduction band states filled by the electrons from the metal donor dopants. From simple electron–phonon scattering, the electrical resistivity should then follow a linear temperature-dependence for $T \gg \Theta_D$, Θ_D being the Debye temperature [21–23]. Θ_D was determined from intersection of extrapolated tangential lines of two different slopes of $d\rho/dT$ between high- and low-temperature regions. Using the data from Fig. 2(a), samples with $x=0.7\%$, 3.2%, 4.2%, and 9.1%, the values of Θ_D are 195, 210, 163, and 185 K, respectively, as tabulated in Table 1 for future comparisons. These similar Debye temperatures suggest that the overall integrity of the lattice has not been altered within the Nb-doping range.

The Hall mobility of charge carriers, given in Fig. 2(c) shows a negative $d\mu_H/dT$, most obviously for $x=3.2\%$. This small temperature dependence, in line with the degenerate semiconductor behavior, possibly reflects the dominance of charge-carrier scattering by ionized and neutral impurities in the degenerate limit [24,25]. The ionized centers are thought to be O vacancies, or substitutional atoms of Nb, while excessive dopants not contributing any carriers are largely neutral, though possibilities of In vacancies, O and Nb interstitials cannot be completely ruled out. But, at any rate, the sample with $x=3.2\%$ has the highest mobility of $\mu_H(300\text{ K})=17.4\text{ cm}^2\text{ V}^{-1}\text{ s}^{-1}$, or about 40% lower than that of the reported $29\text{ cm}^2\text{ V}^{-1}\text{ s}^{-1}$ for commercial ITO [12–14,26]. For Zr-doped In_2O_3 the highest mobility is $110\text{ cm}^2\text{ V}^{-1}\text{ s}^{-1}$, while for sputtered ITO thin films, it is $\sim70\text{ cm}^2\text{ V}^{-1}\text{ s}^{-1}$ [27]. An intrinsic limit of $90\text{ cm}^2\text{ V}^{-1}\text{ s}^{-1}$ has been estimated for ITO [28]. Higher mobilities of $150\text{ cm}^2\text{ V}^{-1}\text{ s}^{-1}$ [29] and $110\text{ cm}^2\text{ V}^{-1}\text{ s}^{-1}$ [30], have also been reported for polycrystalline and epitaxial In_2O_3 films, respectively. The lower mobilities observed in our case could be attributed to the use of Ar as the only sputtering gas, which could likely produce oxygen-deficient films of ample charge-scattering centers. The reported Sn-doped [27] and Mo-doped [31] films were prepared using mixtures of Ar and O_2 with which oxidation could have taken place to reduce the number of oxygen vacancies and, therefore, increase the mobility.

3.3. Optical properties

Fig. 4(a) shows the optical transmission after subtracting the YSZ-substrate contributions and normalized to a thickness of 200 nm for general comparison. Here

$$T_{film} = \exp(-\alpha d) \tag{3}$$

d being the film thickness and α the optical absorption coefficient. The transmittance is greater than 97% in the visible spectral region from 450 to 700 nm, from which the optical absorption coefficients at $\lambda=500$ nm are found to range from 500 to 2400 cm^{-1}. The transparency level, achieved for the whole range of doping levels, is higher than reported values of 90% for

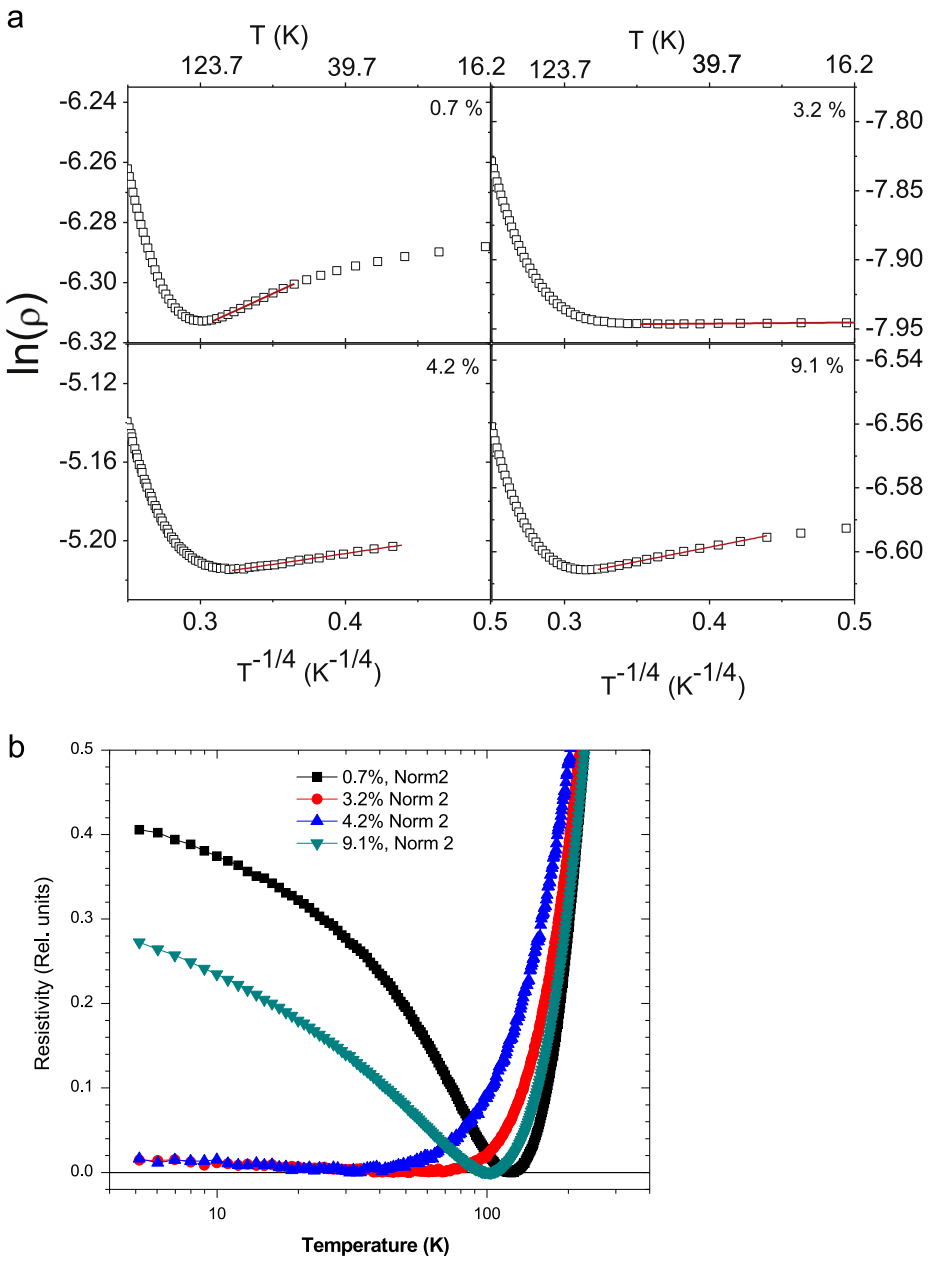

Fig. 3. Analysis of low temperature resistivity region by (a) variable range hopping (VRH). The fitting uses a three dimensional model; (b) plot vs. log$T$ for comparison with weak localization [16].

commercial ITO [13], though higher values have also been asserted by various sources without mention of calibrations, and 85% for experimental Ga:ZnO [9]. The NIR transmittance did not change drastically with x, except for the sample of $x=3.2\%$. However, for doped samples the transmittance values were largely lower than that for the undoped In_2O_3, reflecting higher concentrations of free carriers in the conduction band for doped samples.

The optical band gaps were calculated from the linear functional dependence of α^2 vs. $h\nu$ based on a direct band gap semiconductor model [32], where a linear extrapolation was applied to the optical absorption coefficients α in the spectral region with $\alpha > 10^7\ cm^{-1}$ to obtain the intercept of photon energy where $\alpha=0$. This energy value does not necessarily speak for a true energy gap related to the intrinsic In_2O_3 semiconductor, which has been a subject of recent debate [33–35], but by comparing the change of optical band gap based on the same extrapolation, one may determine the change of Fermi energy as a function of doping level for a degenerate semiconductor such as the In_2O_3 studied here. The inset of Fig. 4(a) shows the optical band gap plotted with respect to $n_{Hall}^{2/3}$, n is the carrier concentration from the Hall measurement. This linear functional dependence at $T=300\ K$ is consistent with the Burstein–Moss shift arguments in the context of nearly-free electron model under the Fermi statistics [32] for a degenerate n-type semiconductor. The increase of optical band gap associated with increasing Nb-doping level is due to the rise of density of charge carriers in the conduction band that causes an up-shift of the Fermi level. The measured optical band gap of the sample without intentional Nb doping ($x=0\%$) is 3.66 eV, which corresponds to $n_{Hall}=1.77\times10^{20}\ cm^{-3}$, indicating that this set of samples are heavily doped even before the introduction of Nb. This high concentration of carriers is a manifestation of inherent defects in the supposedly intrinsic semiconductor. By extrapolating the

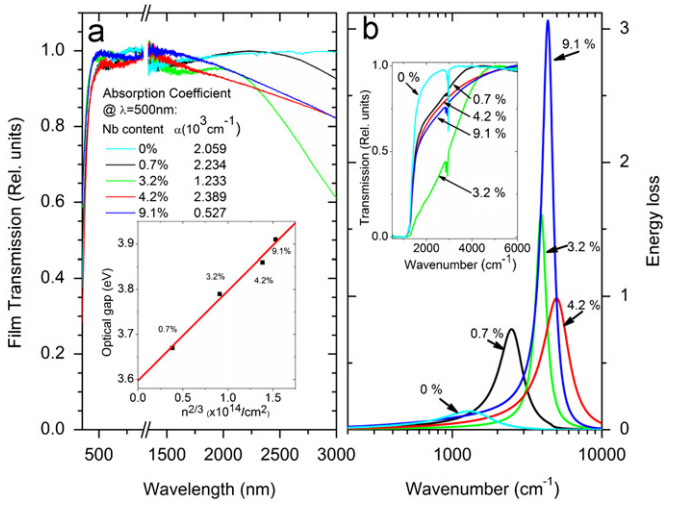

Fig. 4. (a) Optical UV–vis and IR transmission as a function of wavelength for film thickness of 200 nm calculated with Eq. (3). The absorption coefficients are given for $\lambda=500$ nm. Inset: the optical energy gap as a function of $n(300\ \mathrm{K})^{2/3}$. (b) Energy loss as a function of wavenumber. Inset: Optical IR transmission as a function of wavenumber. The color scheme applies for all graphs.

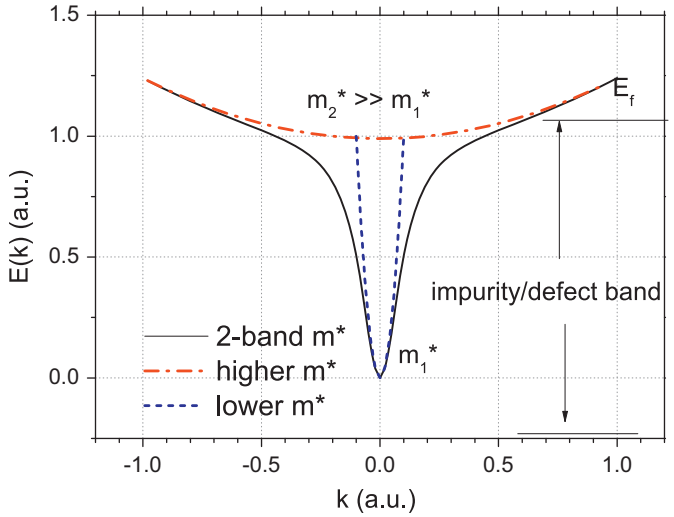

Fig. 5. Sketch of conduction band of the host semiconductor with dual-band overlap with the impurity states.

optical gaps vs. $n_{\mathrm{Hall}}^{2/3}$ values to $n=0$, as shown in the inset of Fig. 4(a), would give $E_o=3.58\pm0.01$ eV, which is consistent with the reported value for In_2O_3 [31]. The Fermi level for the sample with $x=0\%$ is thus $E_f=3.66-3.58=0.08$ eV. The small value of E_f in association with a high value of $n_{\mathrm{Hall}}=1.77\times10^{20}$ cm^{-3}, however, implies an unusually large effective mass $m^*\approx1.44m_e$ calculated with [32]

$$E_f=\hbar^2(3\pi^2n)^2/2m^* \tag{4}$$

from a simple nearly-free-electron point of view. But in this view, if $m^*=0.35m_e$ as taken from literature [2], then $E_f=0.33$ eV, and the true band gap of a truly intrinsic In_2O_3 host semiconductor would consequently be $E_g=3.66-0.33=3.33$ eV, 0.25 eV smaller than the 3.58 eV mentioned above. This inconsistency is reconciled below based on the plasma frequency measurement that gives the ratio n/m^* using infrared reflection or transmission spectroscopy.

Fig. 4(b) shows the energy loss functions of thin films as extracted from the FTIR-transmittance data in the range 500–6000 cm^{-1}, viz. $-Im\{1/\tilde{\varepsilon}\}=\varepsilon_2/(\varepsilon_1^2+\varepsilon_2^2)$, where $\tilde{\varepsilon}=\varepsilon_1+i\varepsilon_2$ is the complex dielectric constant, which can be analyzed by simulation using the SCOUT software [36] with an extended Drude model [37–39]. Note that the plasma frequency is calculated as [36]:

$$\int -\omega Im(1/\tilde{\varepsilon})\,d\omega=\pi\omega_p^2/2 \tag{5}$$

with the plasma frequency

$$\omega_p^2=\frac{n_{\mathrm{opt}}e^2}{\varepsilon_0\varepsilon_\infty m^*} \tag{6}$$

where n_{opt} is defined as optical free carriers in distinction with the Hall carrier concentration, n_{Hall}. The extraction of n_{opt} assumed $\varepsilon_\infty=4$ and $m^*=0.35m_e$ [2] as noted in Table 1, showing consistent increase in the concentration of free carriers with increasing nominal Nb-doping. The optical carrier mobility, calculated from the plasma damping, was obtained based on zero-frequency damping coefficient [37], as is also summarized in Table 1.

The inconsistency between n_{Hall} and n_{opt} calls for a further look at the effective electron mass m^*. First, by measuring ω_p one obtains the ratio n_{opt}/m^* [38], from which n_{opt} can be calculated with a given m^* that is assumed constant. However, if using what is commonly quoted as $m^*=0.35m_e$ [2] in Eq. (6), the discrepancy between n_{Hall} and n_{opt} is as large as 10 in their ratio of $n_{\mathrm{Hall}}/n_{\mathrm{opt}}$ which implies an effective mass $m^*\gg0.35m_e$ in the conduction band. This raises a question about the legitimacy of assuming a constant effective mass in simple parabolic band structure of free-electron-like metals [40]. To resolve this inconsistency, we propose the existence of a deeper valley in which for pure In_2O_3 semiconductors the effective mass is still on order of $0.35m_e$, [2], and $E_g=3.33$ eV as calculated earlier. This deep-valley band may overlap with the impurities states, which could have either already formed into a continuous band due to the high density of defect states, or remain discrete but densely populated in the k-space. But, either way, in this scenario, the host semiconductor would remain metal-like as the deep-valley states are already filled. If taking $E_g=2.9$ eV, instead of the 3.58 eV mentioned earlier [29], as suggested for In_2O_3 by some authors [33–35], then for the sample with $x=0\%$ $E_f=E_o-E_g=3.66-2.9=0.76$ eV. By substituting the E_f into Eq. (4) and letting $n=n_{\mathrm{Hall}}$, one has $m^*=0.15m_e$. This smaller effective-mass band, as sketched in Fig. 5, in the two-band model thus could properly reconcile the inconsistency of two measurements, though the model assumes that $E_g=2.9$ eV.

3.4. Evidence of Nb_2O_4 formation based on X-ray photoemission spectroscopy (XPS)

The XPS data of the thin films, as shown in Fig. 6, give no sign of elemental Nb, based on the spin–orbit split peaks of Nb $3d_{3/2}$ and $3d_{5/2}$ for the doped samples, thus excluding the possibilities of Nb metal segregation. With reference to the In $3d_{5/2}$ and $3d_{3/2}$ peaks, which come with a spin–orbit splitting of 7.6 eV, and are located at binding energies of (B.E.) of 443.9 and 451.5 eV, respectively, the Nb $3d_{5/2}$ and $3d_{3/2}$ peaks with spin–orbit splitting of ~2.7 eV are accordingly identified with their B.E. at 206.4 and 209.2 eV, respectively [41–48]. These B.E. values reflect the valence state of Nb^{4+}, namely, bonding of type Nb_2O_4, for all doped thin films. No Nb oxidation states other than $n=4$ are identified as Nb^{n+} for $n=0$, 2, 3 and 5 has the Nb $3d_{5/2}$ B.E. located at 202.4, 203.7, 203.5 and 207.8 eV, respectively. Charge screening effect is not considered herein, nonetheless, because peak separation is used for comparison and screening effects, if significant, are considered to be imposed similarly for all charge states in various samples. There seem to be no change of binding

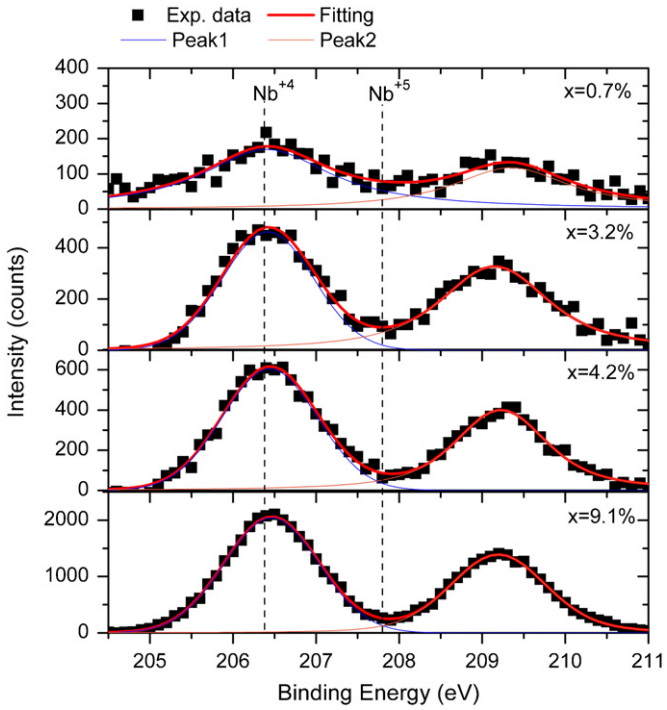

Fig. 6. XPS profile of Nb binding energy for all doped samples, suggesting the bonding state of Nb_2O_4. Reference lines for B.E. of $3d_{5/2}$ Nb^{+4} and Nb^{+5} are shown.

energies for different levels of doping up to the highest 9.1% investigated.

The averaged efficiency of Nb-doping (η), defined as the number of free charge carriers per Nb-dopant at room temperature, was estimated using $\eta=[n(300\text{ K},\ x)-n(300\text{ K},\ 0\%)]/[\text{Nb-atoms introduced}]$ to give $\eta=26\%$, 66%, 97%, and 59% for Nb-doping $x=0.7\%$, 3.2%, 4.2%, and 9.1%, respectively. Note that the shift of the energy loss function peak vs. Nb-doping is consistent with the Nb-doping efficiency in sequence of $\eta_{0.7\%}<\eta_{9.1\%}<\eta_{3.2\%}<\eta_{4.2\%}$, see Fig. 4(b). The 9.1% anomaly may be attributed to heavy oxometalate formation due to heavy doping [49]. That the maximum doping efficiency was $\eta=97\%$ can be interpreted as essentially the loss of more than half of the Nb doped into the host In_2O_3 in their function as a donor due to the formation of Nb_2O_4. This formation is likely to arise from the formation of Nb–O oxometalates in the host In_2O_3 which localize the valence electrons initially intended as free carriers [49]. However, this by no means suggests that oxometalates have to exist as molecular clusters, as they could simply be oxygen interstitials (O_i) attracted to Nb_{In} resulting effectively as a molecule with composition of Nb_2O_{3+x} nearby the Nb_{In} substitutional site, with $x=1$ as shown with the XPS data. Compensation of charge carriers may take place as an oxygen atom is drawn into interstitial sites near Nb_{In} whereby the O_i atom would act as a stringent charge trap if bonded to Nb_{In}, or, to a lesser degree, as a shallow trap if forming a weaker complex with the Nb_{In} atom. Either way, an O_i" takes two charges to fully fill its available orbital states. However, if only loosely attracted, the O_i atom may remain neutral or partially charged, i.e., $O_i^{-(2-\delta)}$, by freeing up a fraction δ of two charges from Nb, thus leading to a reduced doping efficiency since there will only be δ electrons ($\delta\leq 2$) to contribute to the pool of free carriers. Meanwhile, vacancies of In (V_{In}) or In interstitials (In_i), which could be charged, may also exist and play some key roles in contributing to the reduced η. But, in all, the effect of Nb-doping on the eventual transport behaviors depends on where the dopants go into the host In_2O_3 lattice, as point defects and formations of molecular or atomic oxometalate, or V_O left behind from oxygen drawn to the oxometalate, would all affect the eventual free carrier concentration.

What we have discussed above inherently involve complicated formation of point defects, a subject that remains extremely challenging to grasp as such defects frequently evaded detection even under close scrutiny of contemporary instruments; hence often no conclusion can be drawn without some element of speculation. In the present case, it remains an unsettled issue as to what is responsible, if not V_O, for the n-doping. In the literature various other point defects are still being considered to be the origins [41,42,44,45,47,48]. A first principle calculation showed that V_O was too far from the conduction band minimum to be an effective donor [41]. Judged from the electrical, optical properties and the XPS chemical analysis, however, we think that V_O still plays at least an associate role in the donor doping process as it may be associated with the existence of In_i or O_i interstitials [45], like when oxygen atoms on the host lattice (O_O) are drawn into O_i sites near Nb_{In}, In_i or Nb_i interstitial sites to form chemical bonds or complexes of oxometalates.

The existence of O_i or In_i near the Nb_{In} sites helps to keep the unit cell size of the In_2O_3 host intact. This is in agreement with the XRD measurement of lattice constants, which were found independent of the Nb doping level. That the lattice constant does not change is indeed surprising considering the Nb atomic and ionic sizes being substantially smaller than those of In [49]. Formation of Nb_2O_4 oxometalates by drawing O_i atoms into interstitial sites nearby a Nb atom accounts for this outcome since the larger sizes of oxometalate compensate for the size difference between the host In atoms and Nb substituent. However, we must point out that such continual formation of the oxometalates seems to at the same time improve the crystal quality to certain extent, as judged by the decrease in broadness, though small, of the rocking curves also given in Table 1. The physical picture portrayed above is not different from what is described in literature for Zn or Sn doped into In_2O_3 in the context of the Frank–Köstlin type of clusters [50] also within the In_2O_3 as a host semiconductor. Concerning the coordination of local atoms, however, it is difficult to pinpoint the local building blocks as tetrahedral, since even if they are, the tetrahedral units could be distorted ones.

4. Summary

Epitaxial thin films of Nb-doped In_2O_3 have been fabricated by co-sputtering of In_2O_3 and Nb targets onto (001)-oriented YSZ substrates with $[001]In_2O_3||[001]YSZ$ and $[110]In_2O_3||[110]YSZ$ aligned to within $\sim$0.41–0.31° based on the rocking width $\Delta\omega$ (FWHM). Hall measurements show the doped films are degenerate semiconductors, where 3.2 at% Nb-doping results in the lowest electrical resistivity with $\rho(300\text{ K})=4.1\times10^{-4}\,\Omega$ cm. These Nb-doped films exhibited a change from positive to negative TCR as temperature was lowered. A rough estimation of the Debye temperature suggests the integrity of the lattice is not altered in the range of Nb-doping. The optical transparencies of the films are mostly greater than 97% in the visible range and the optical band gap blue-shifts with higher dopant concentration, consistent with the Burstein–Moss scenario for degenerate semiconductors. Average doping efficiency of Nb is up to $\sim$1 electron/Nb atom. This maximal doping efficiency is corroborated by the XPS measurement, indicating that most of Nb exist in form of Nb_2O_4, that is, out of the five available valence electrons, four contribute to chemical bonding and only one as free carrier. Other n-doping effect may come from the resulted oxygen vacancies left behind by the oxygen drawn away to form the Nb_2O_4. FTIR measurement as analyzed by a simulation of the dielectric functions shows the doping efficiency is reflected in the plasma

frequency as judged by its consistent shift of the optical energy loss function. The discrepancy between Hall and optical data is suggested as being due to the band structure effects of the host In_2O_3 semiconductor near the conduction band edge.

Acknowledgments

This work was supported in part by the National Science Foundation under Grant no. DMR-0404542, the Department of Energy through Grant no. DE-FG02-05ER46208, the US Air Force of Scientific Research (AFOSR) and the State of Texas Strategic Partnership for Research in Nanotechnology (SPRING) through the Texas Center for Superconductivity at the University of Houston (TCSUH) under Grant no. FA-9550-06-1-0401. Work at National Sun Yat-Sen University (NSYSU) was supported by the Ministry of Education and the National Science Council of Taiwan, Republic of China, under Grant no. 99-2112-M-110-012-MY2 and through the Center for Nanoscience and Nanotechnology at NSYSU. Partial Support by the Taiwan–US Research Partnership through the NSC and AFOSR is also acknowledged. We thank X.M. Wang (TCSUH), W.Y. Pang and the crew of the High Magnetic Field Laboratory (NSYSU) for the untiring technical assistance.

References

[1] D.S. Gingley, C. Bright, Transparent conducting oxides, MRS Bulletin 25 (2000) 15–18.
[2] I. Hamberg, C.G. Granqvist, Evaporated Sn-doped In_2O_3 films: basic optical properties and applications to energy-efficient windows, Journal of Applied Physics 60 (1986) R123–R159.
[3] R.B.H. Tahar, T. Ban, Y. Ohya, Y. Takahashi, Tin doped indium oxide thin films: electrical properties, Journal of Applied Physics 83 (1998) 2631–2645.
[4] M. Yang, J. Feng, G. Li, Q. Zhang, Tungsten-doped In_2O_3 transparent conductive films with high transmittance in near-infrared region, Journal of Crystal Growth 310 (2008) 3474–3477.
[5] T. Koida, M. Kondo, High-mobility transparent conductive Zr-doped In_2O_3, Applied Physics Letters 89 (2006) 082104-1–082104-3.
[6] R.E. Presley, D. Hong, H.Q. Chiang, C.M. Hung, R.L. Hoffman, J.F. Wager, Transparent ring oscillator based on indium gallium oxide thin-film transistors, Solid-State Electronics 50 (2006) 500–503.
[7] D. Craciun, G. Socol, N. Stefan, M. Miroiu, V. Craciun, Structural investigations of InZnO films grown by pulsed laser deposition technique, Thin Solid Films 518 (2010) 4564–4567.
[8] Y. Furubayashi, T. Hitosugi, Y. Yamamoto, K. Inaba, G. Kinoda, Y. Hirose, T. Shimada, T. Hasegawa, A transparent metal: Nb-doped anatase TiO_2, Applied Physics Letters 86 (2005) 252101–252103.
[9] V. Bhosle, A. Tiwari, J. Narayan, Metallic conductivity and metal–semiconductor transition in Ga-doped ZnO, Applied Physics Letters 88 (2006) 032106-1–032106-3.
[10] O. Bamiduro, H. Mustafa, R. Mundle, R.B. Konda, A.K. Pradhan, Metal-like conductivity in transparent Al:ZnO films, Applied Physics Letters 90 (2007) 252108-1–252108-3.
[11] E.J. Tarsa, J.H. English, J.S. Speck, Pulsed laser deposition of oriented In_2O_3 on (001) InAs, MgO, and yttria-stabilized zirconia, Applied Physics Letters 62 (1993) 2332–2334.
[12] J.R. Bellingham, W.A. Philips, C.J. Adkins, Electrical and optical properties of amorphous indium oxide, Journal of Physics Condensed Matter 2 (1990) 6207–6221.
[13] M. Chen, Z.L. Pei, X. Wang, Y.H. Yu, X.H. Liu, C. Sun, L.S. Wen, Intrinsic limit of electrical properties of transparent conductive oxide films, Journal of Physics D: Applied Physics 33 (2000) 2538–2548.
[14] E. Fortunato, P. Barquinha, A. Pimentel, A. Gonçalves, A. Marques, L. Pereira, R. Martins, Recent advances in ZnO transparent thin film transistors, Thin Solid Films 487 (2005) 205–211.
[15] T. Minami, New n-type transparent conducting oxides, MRS Bulletin 25 (2000) 38–44.
[16] M. Nistor, F. Gherendi, N.B. Mandache, C. Hebert, J. Perriere, W. Seiler, Metal–semiconductor transition in epitaxial ZnO thin films, Journal of Applied Physics 106 (2009) 103710–103717.
[17] M. Nistor, N.B. Mandache, J. Perrière, C. Hebert, F. Gherendi, W. Seiler, Growth, structural and electrical properties of polar ZnO thin films on MgO (100) substrates, Thin Solid Films 519 (2011) 3959–3964.
[18] P.A. Lee, T.V. Ramakrishnan, Disordered electronic systems, Reviews of Modern Physics 57 (1985) 287–337.
[19] N.F. Mott, Conduction in non-crystalline materials III. Localized states in a pseudogap and near extremities of conduction and valence bands, Philosophical Magazine 19 (1969) 835–852.
[20] O.M. Berengue, C.A. Amorim, H. Kamimura, A.J. Chiquito, E.R. Leite, Oxygen-induced metal–insulator-transition on single crystalline metal oxide wires, Journal of Applied Physics 111 (2012) 013713-1–013713-6.
[21] N.W. Ashcroft, N.D. Mermin, Solid State Physics, Brooks/Cole, Pacific Grove, California, New Jersey, 1976. pp. 458–461.
[22] G. Burns, Solid State Physics, Academic Press, London, 1985. (Chapter 11).
[23] C. Kittel, Introduction to Solid State Physics, eighth ed., John Wiley and Sons, New York, 2005, pp.112–114.
[24] D.L. Dexter, F. Seitz, Effects of dislocations on mobilities in semiconductors, Physical Review 86 (1952) 964–965.
[25] H.L. Hartnagel, A.L. Dawar, A.K. Jain, C. Jagadish, Semiconducting Transparent Thin Films, Taylor & Francis, Bristol, 1995. pp. 138–143.
[26] M.F.A.M. Van Hest, M.S. Dabney, J.D. Perkins, D.S. Gingley, M.P. Taylor, Titanium-doped indium oxide: a high-mobility transparent conductor, Applied Physics Letters 87 (2005) 032111–032113.
[27] D. Mergel, M. Schenkel, M. Ghebre, M. Sulkowski, Structural and electrical properties of In_2O_3:Sn films prepared by radio-frequency sputtering, Thin Solid Films 392 (2001) 91–97.
[28] J.R. Bellingham, W.A. Phillips, C.J. Adkins, Intrinsic performance limits in transparent conducting oxides, Journal of Materials Science Letters 11 (1992) 263–265.
[29] H. Nakazawa, Y. Ito, E. Matsumoto, K. Adachi, N. Aoki, Y. Ochiai, The electronic properties of amorphous and crystallized In_2O_3 films, Journal of Applied Physics 100 (2006) 093706–093708.
[30] T. Koida, M. Kondo, High electron mobility of indium oxide grown on yttria-stabilized zirconia, Journal of Applied Physics 99 (2006) 123703–123706.
[31] Y. Yoshida, T.A. Gessert, C.L. Perkins, T.J. Coutts, Development of radio-frequency magnetron sputtered indium molybdenum oxide, Journal of Vacuum Science and Technology A 21 (2003) 1092–1097.
[32] J.I. Pankove, Optical Processes in Semiconductors, second ed., Dover Publishers, New York, 1975. p. 35.
[33] A. Walsh, J.L.F.D. Silva, S.-H. Wei, C. Körber, A. Klein, L.F.J. Piper, A. DeMasi, K.E. Smith, G. Panaccione, P. Torelli, D.J. Payne, A. Bourlange, R.G. Egdell, Nature of the band gap of In_2O_3 revealed by first-principles calculations and X-ray spectroscopy, Physical Review Letters 100 (2008) 167402–167404.
[34] P.D.C. King, T.D. Veal, F. Fuchs, C.Y. Wang, D.J. Payne, A. Bourlange, H. Zhang, G.R. Bell, V. Cimalla, O. Ambacher, R.G. Egdell, F. Bechstedt, C.F. McConville, Band gap, electronic structure, and surface electron accumulation of cubic and rhombohedral In_2O_3, Physical Review B 79 (2009) 205211-1–205211-10.
[35] R.L. Weiher, R.P. Ley, Optical properties of indium oxide, Journal of Applied Physics 37 (1966) 299–302.
[36] W. Theiss, Hard- and Software Dr.-Bernhard-Klein-Str. 110, D-52078 Aachen, Germany. ⟨www.mtheiss.com⟩.
[37] D. Mergel, Z. Qiao, Dielectric modelling of optical spectra of thin In_2O_3:Sn films, Journal of Physics D: Applied Physics 35 (2002) 794–801.
[38] T. Pisarkiewicz, K. Zarkzewska, E. Leja, Scattering of charge carriers in transparent and conducting thin oxide films with a non-parabolic conduction band, Thin Solid Films 174 (1989) 217–223.
[39] F. Wooten, Optical Properties of Solids, Academic Press, New York, 1972, pp. 79–80.
[40] Y. Furubayashi, N. Yamada, Y. Hirose, Y. Yamamoto, M. Otani, Transport properties of d-electron-based transparent conducting oxide: anatase $Ti_{1-x}Nb_xO_2$, Journal of Applied Physics 101 (2007) 093705-1-093705-5.
[41] S. Lany, A. Zunger, Dopability, intrinsic conductivity, and nonstoichiometry of transparent conducting oxides, Physical Review Letters 98 (2007) 045501-1–045501-4.
[42] C.G. Li, Y. Gao, N. Dong, Study on composition in niobium anode, Journal of Electronics (China) 21 (2004) 437–440.
[43] J.F. Moulder, W.F. Stickle, P.E. Sobol, K.P. Bomben, Handbook of X-ray Photoelectron Spectroscopy, Physical Electronics Inc., Minnesota, 1992.
[44] H. Nogawa, A. Chikamatsu, Y. Hirose, S. Nakao, H. Kumigashira, M. Oshima, T. Hasegawa, Carrier compensation mechanism in heavily Nb-doped anatase $Ti_{1-x}Nb_xO_{2+\delta}$ epitaxial thin films, Journal of Physics D: Applied Physics 44 (2011) 365404-1–365404-6.
[45] T. Ohsawa, J. Okubo, T. Suzuki, H.I. Kumigashira, M. Oshima, T. Hitosugi, An n-type transparent conducting oxide: $Nb_{12}O_{29}$, Journal of Physical Chemistry C 115 (2011) 16625–16629.
[46] C.A. Pan, T.P. Ma, Highly-quality transparent conductive indium oxide films prepared by thermal evaporation, Applied Physics Letters 37 (1980) 163–165.
[47] L.-M. Tang, L.-L. Wang, D. Wang, J.-Z. Liu, K.-Q. Chen, Donor–donor binding in In_2O_3: engineering shallow donor levels, Journal of Applied Physics 107 (2010) 083704-1–083704-5.
[48] T. Tomita, K.I. Yamashita, Y. Hayafuji, The origin of n-type conductivity in undoped In_2O_3, Applied Physics Letters 87 (2005) 051911–051913.
[49] F.A. Cotton, G. Wilkinson, C.A. Murillo, M. Bochmann, Advanced Inorganic Chemistry, sixth ed., John Wiley, New York, 2003, pp. 895–898.
[50] G. Frank, H. Köstlin, Electrical properties and defect model of tin-doped indium oxide layers, Applied Physics A 27 (1982) 197–206.